Dependence of Current and Field Driven Depinning of Domain Walls on Their Structure and Chirality in Permalloy Nanowires

Masamitsu Hayashi,[1,2] Luc Thomas,[1] Charles Rettner,[1] Rai Moriya,[1] Xin Jiang,[1] and Stuart S. P. Parkin[1,*]

[1]*IBM Almaden Research Center, San Jose, California, USA*

[2]*Department of Materials Science and Engineering, Stanford University, Stanford, California, USA*

(Received 2 January 2006; published 16 November 2006)

A magnetic domain wall (DW) injected and pinned at a notch in a permalloy nanowire is shown to exhibit four well-defined magnetic states, vortex and transverse, each with two chiralities. These states, imaged using magnetic force microscopy, are readily detected from their different resistance values arising from the anisotropic magnetoresistance effect. Whereas distinct depinning fields and critical depinning currents in the presence of magnetic fields are found, the critical depinning currents are surprisingly similar for all four DW states in low magnetic fields. We observe current-induced transformations between these DW states below the critical depinning current which may account for the similar depinning currents.

DOI: 10.1103/PhysRevLett.97.207205 PACS numbers: 75.60.Ch, 72.25.Ba, 75.75.+a

The manipulation of magnetic domain walls (DW) in nanowires has attracted much interest recently, with proposals for prospective logic [1] and memory devices [2]. In these devices, information is encoded in the magnetic states of domains in lithographically patterned nanowires. DW motion along the wires allows for the access and manipulation of the stored information. Whereas magnetic fields have been conventionally used to manipulate DWs, it has recently been shown that a spin polarized current can also cause DW motion by acting as a source of spin angular momentum [3–18]. However, this mechanism is poorly understood, especially with regard to the detailed magnetic structure of the DW. In this Letter, we study the current and field-induced depinning of DWs of different structures from the same notch in a permalloy nanowire and show that, surprisingly, in small magnetic fields the critical current is insensitive to the DW structure.

Magnetic nanowires, 100 to 300 nm wide, are formed from 10 nm thick permalloy ($Ni_{81}Fe_{19}$) films deposited on highly resistive Si(100) substrates by magnetron sputtering. The nanowires are fabricated by electron beam lithography and Ar ion milling. Contact lines are made by patterning 5 nm Ta/45 nm Rh films, subsequently deposited on top of the nanowires. A scanning electron microscopy (SEM) image of a typical nanowire is shown in Fig. 1(a). The distance between the two contact lines, labeled A and B, is 4 μm. Both ends of the nanowire are tapered to a sharp point to prevent the formation of DWs outside the contact lines [19]. High frequency probes are used to inject nanosecond long pulses along the nanowire and to measure the dc resistance of the wire. In this Letter detailed results are presented for a 300 nm wide nanowire in which a triangularly shaped notch, whose depth is $\sim$30% of the wire width, is patterned along one edge. The dimensions of the nanowire are chosen so that a number of metastable DW states coexist.

The following procedure is used to inject a DW into the wire [20,21]. (1) The nanowire is first magnetized along the x axis by applying a large in-plane magnetic field $H_{SAT} = -270$ Oe [see Fig. 1(a) for definition of x]. (2) A magnetic field, termed the injection field H_{INJ} hereafter, is applied in a direction opposite to H_{SAT} to assist the nucleation and subsequent propagation of the DWs. (3) With H_{INJ} turned on, a voltage pulse, 2.1 V in amplitude and 10 ns long, is passed along contact line A. The pulse generates a local magnetic field sufficiently large ($\sim$200 Oe) to reverse the magnetization direction of the portion of the nanowire that is located immediately underneath the line, so forming two DWs. H_{INJ} will cause the two DWs to move in opposite directions, one moving towards the notch, and the other moving towards the wire's pointed end. If H_{INJ} does not exceed the pinning field of the notch, one DW will consequently be trapped at the notch. The other DW will be annihilated at the pointed end. (4) H_{INJ} is set to zero.

Because of the anisotropic magnetoresistance (AMR) of permalloy the presence of a DW lowers the resistance of the nanowire [22,23]. Since this effect is small the resistance of the nanowire R is compared to that of its magnetized state R_{SAT}, each measured in zero field. The presence of a DW in the region between contact lines A and B is thereby detected from the resistance change $\Delta R = R - R_{SAT}$. As an example, Fig. 1(b) plots the values of ΔR for a succession of measurements in which steps (1)–(4) are repeated many times, using $H_{INJ} = 12$ Oe. A histogram of ΔR for a complete set of these measurements is plotted in Fig. 1(c). In each case, ΔR is negative, consistent with AMR, but its magnitude varies. For $H_{INJ} = 12$ Oe, there are four unambiguous ΔR peaks. Histograms of ΔR using different H_{INJ} values to inject the DW are plotted in Fig. 1(d). For H_{INJ} larger than 4 Oe, the same four main peaks are observed whose ΔR values are independent of H_{INJ} (note that the peak around $\Delta R \sim 0$ corresponds to

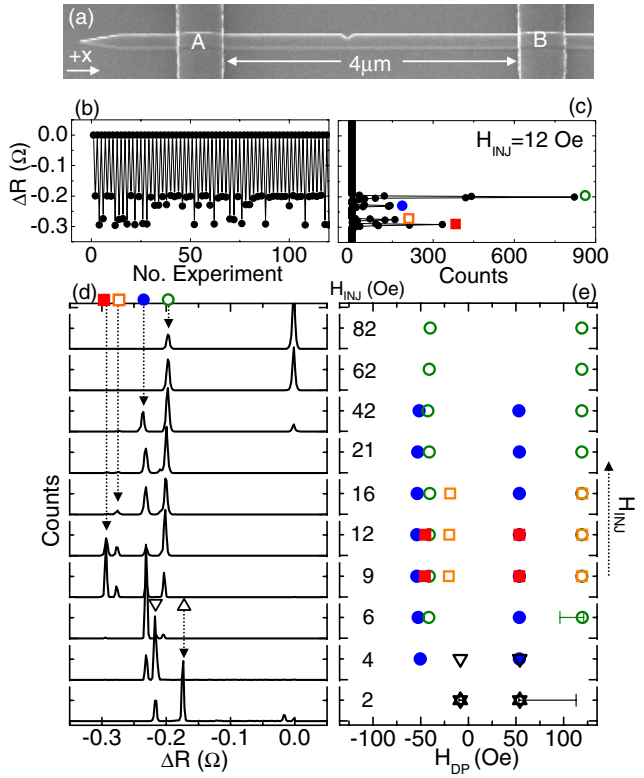

FIG. 1 (color online). (a) SEM image of the permalloy nanowire. A and B are electrical contact lines (Ta/Rh). (b) Measurements of ΔR in a series of experiments in which the wire is first magnetized ($\Delta R = 0$) and a DW is subsequently injected with an injection field $H_{\mathrm{INJ}} = 12$ Oe. (c) Histogram of ΔR values from (b). Note that only a subset of these data are shown in (b). (d) Histogram of ΔR values for different H_{INJ}. Values of H_{INJ} are shown in (e). Symbols indicate different DW states. (e) Depinning fields for each DW state observed in (d). Symbols correspond to those shown in (d). The vertical axis represents the magnitude of the injection field with arbitrary spacing.

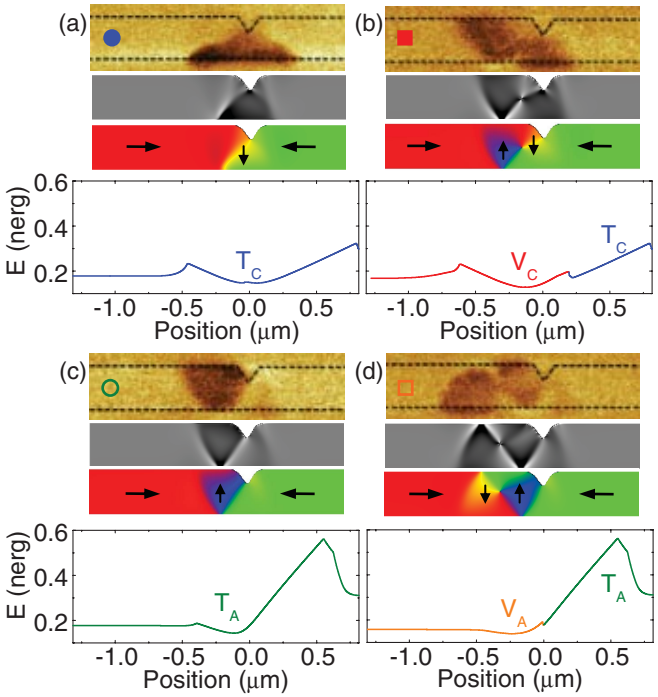

FIG. 2 (color). Each of the four panels (a)–(d), corresponding to the four distinct ΔR states of Fig. 1(c), contain, from top to bottom: (1) MFM image [the symbols shown at the left side correspond to those in Fig. 1(d)]. Micromagnetic simulations of the divergence (2) and the direction (3) of the magnetization. (4) Calculated energy of the DW versus position along the nanowire. The state of the DW is indicated by the line color and the label. Note that V_C (V_A) walls transform to T_C (T_A) walls when the DW is moved across the notch to the right.

states where no DW formed). However, the relative size of the peaks varies with H_{INJ}. Thus, the number of accessible DW states can be varied by tuning H_{INJ}. Below 4 Oe, both the number and position of the peaks changes abruptly, as discussed later.

Magnetic force microscopy (MFM) imaging experiments show that the ΔR peaks in Fig. 1(d) correspond to four distinct DW states. ΔR is measured before and after MFM imaging to confirm that the state of the DW is not altered by stray fields from the MFM tip. The MFM images are compared with micromagnetic simulations [24] to identify the corresponding DW structures (see Fig. 2). Excellent agreement is obtained between the simulated and experimental images, allowing us to identify the four states as (a) transverse wall located in the notch (solid circles, labeled as T_C hereafter), (b) vortex wall located in the notch (solid squares, V_C), (c) transverse wall located at one side of the notch (open circles, T_A), and (d) vortex wall located at one side of the notch (open squares, V_A). Note that since the DWs are injected from the left side of the notch, i.e., from contact line A, they are more likely to be located at the left side of the notch. Interestingly, we find that the *chirality* of the DW determines whether the DW resides inside or to one side of the notch. This is because the energy of the DW is lowered (raised) when the component of its transverse magnetization within the notch is directed away from (to) the notch. We describe the chirality of these DWs as clockwise (T_C and V_C) and anticlockwise (T_A and V_A), respectively.

Further insight into the characteristics of these different DW states is obtained by studying their field-induced depinning from the notch. DWs are injected into the nanowire using steps (1)–(4). The field is then ramped up to a certain value and is reduced to zero to measure ΔR. This process is repeated for fields in the range from -120 Oe to 120 Oe, and is repeated 50 times for each field to obtain a statistical average. We define the depinning field H_{DP} as the minimum field at which the probability that the DW is driven out from the nanowire ($\Delta R = 0$) exceeds 50%. Depinning fields measured for all the DW states listed in Fig. 1(d) are plotted in Fig. 1(e) as functions of the injection field. Error bars (20%–80% depinning probability) are smaller than the symbols except where shown. Interestingly, the depinning fields are nearly independent of H_{INJ}, confirming that states with the same ΔR have the same

magnetic structure. For low injection fields (below ~4 Oe), the depinning field in the negative field direction is close to zero, indicating that the DW is not captured by the notch's potential well, and thus likely did not travel all the way to the notch. These states are indicated by the triangularly shaped symbols in Fig. 1. Thus we conclude that the minimum field needed to move the DW along the nanowire, the propagation field, is ~4–5 Oe.

In the following, we discuss the four DW structures pinned at the notch. From Fig. 1(e), the depinning fields are significantly different for positive and negative fields when the DW is located to one side of the notch, i.e., for anticlockwise DWs (open circles and squares). For example, compare $H_{\mathrm{DP}}^{\mp} = -41$ and $+119$ Oe for V_A walls at $H_{\mathrm{INJ}} = 12$ Oe. In order to further understand the correlation between the DW structure and its depinning field, the notch potentials for the four DW states are calculated from micromagnetic simulations [25], as shown in Fig. 2. The difference in the positive and negative depinning fields can be understood from the asymmetrical shape of the pinning potential. The simulations also show that for the vortex walls, the DW transforms to a transverse state when it is moved across the notch [see Fig. 2(b) and 2(d)]. The depinning fields for each DW state can be extracted from the corresponding energy landscape, which reflects these DW transformations, and match well the experimental values of $H_{\mathrm{DP}}^{\mp}$. For example, for T_C (T_A) walls the experimental and calculated values of $H_{\mathrm{DP}}^{\mp}$ are $-54/54$ Oe ($-44/119$ Oe) and $-56/60$ Oe ($-45/156$ Oe), respectively.

We now consider current-assisted depinning for the different DW states. As above, a DW is injected into the nanowire, with $H_{\mathrm{INJ}} = 12$ Oe, and ΔR is measured in zero field to determine the DW state. Then an external bias field (H_B) is applied along the x direction. In addition, a voltage pulse of 4 ns duration and variable amplitude is applied from line B to A so as to inject a short current pulse into the nanowire. ΔR is measured after the voltage pulse, to determine whether the DW is depinned and ejected from region A-B. Since the pulse generator is a constant voltage source, the actual current density flowing in the nanowire depends upon its resistance which may increase during the pulse due to Joule heating. The nanowire resistance was measured in real time using a sampling oscilloscope (12 GHz bandwidth) and this value was used to infer the actual current density in the nanowire. The temperature reached during the 4 ns long pulse can be estimated from the dc resistance versus temperature relationship measured in a permalloy film of the same thickness (see Fig. 3 and the discussion below).

The critical current density J_C required to depin the DW from the notch is plotted as a function of applied field H_B in Fig. 3 for the four DW structures, for both positive and negative current. J_C represents the minimum current density needed to depin the DW from the notch with a probability greater than 50%. Positive current corresponds to

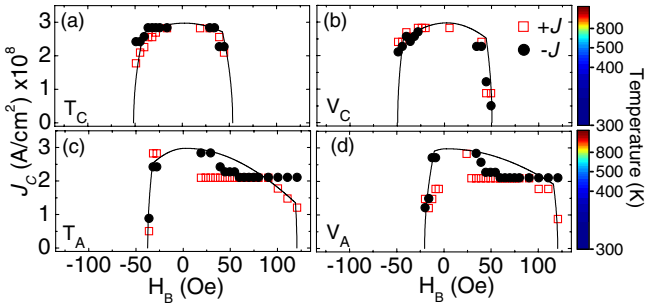

FIG. 3 (color online). Critical current density (J_C) to depin the DW from the notch as a function of applied field H_B for the four states shown in Fig. 1(c). The initial DW structure is indicated in the bottom left corner of each panel. Applied voltage pulses are 4 ns long. Lines are a guide to the eye. Device temperature corresponding to the applied current density is shown at the right side as a color scale.

electrons flowing in the positive x direction in Fig. 1(a). The measured field dependences of J_C show similar characteristics for DWs with the same chirality. For example, T_A and V_A walls show constant J_C over a large range of H_B at high positive fields [compare Fig. 3(c) and 3(d)]. At negative H_B, J_C rapidly increases as H_B is reduced from the depinning field. For T_C and V_C walls, J_C is nearly symmetric with respect to the applied field direction [compare Fig. 3(a) and 3(b)]. For most of the wall structures, the extrapolated J_C at zero field show similar values, i.e., $J_C(0) \sim 3 \times 10^8$ A/cm^2. The device temperature corresponding to the current density is shown as a color scale at the right side of the figure. Note that the temperature (~780 K) at the highest currents needed to depin the DWs near zero applied field approaches the Curie temperature of permalloy [17].

In order to obtain further insight into the current-assisted depinning process, the phase diagrams of the *most probable* resistance level (ΔR) after the application of positive or negative voltage pulses are shown in Fig. 4(a)–4(d) as a function of the applied current density and H_B. Note that the highest voltage pulse used in this plot is 80% of that shown in Fig. 3. The device temperature scale is again indicated by the color scale at the right side of the figure. The initial DW structures are listed at the top left corner of each panel in the figure. To clarify the correspondence between the resistance level and the DW structure, the resistance level is color scaled (see the scale bar at the top of Fig. 4). One can clearly see transitions between different DW structures below J_C. The T_C wall [Fig. 4(a)] appears to be the most stable state against current perturbations. The T_A wall [Fig. 4(c)] transforms to either T_C or V_C at low H_B depending on the direction of current. Vortex walls [Fig. 4(b) and 4(d)] also show transitions to transverse walls at high current density. Thus the wall chirality as well as the basic structure can be changed with current. Note that the V_A wall transforms to a T_A wall without any current when H_B exceeds ~50 Oe, consistent with micro-

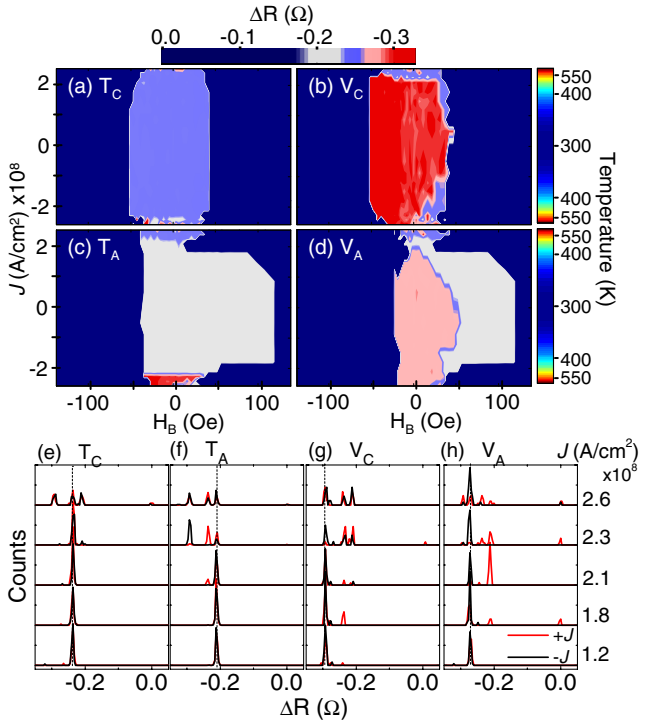

FIG. 4 (color online). (a)–(d) Stability phase diagram for the four DW states. The most probable resistance (ΔR) level after application of a 4 ns long voltage pulses is plotted as a function of current density and H_B. Color scale represents the ΔR level. (e)–(h) Histograms of ΔR values after the application of 4 ns long voltage pulses for the four DW states. The dotted line indicates the initial ΔR level (before the application of the pulse). Counts are normalized by the number of experiments for each DW structure.

magnetic simulations [see Fig. 2(d)]. Interestingly, the current-assisted depinning at high positive H_B for T_A and V_A walls likely involves wall structure transformations, i.e., J_C may represent the current density needed to transform the wall into either the T_C or V_C wall, which is then immediately depinned at these high H_B. We surmise that the current-induced DW transformations are due to vortex core motion induced by spin polarized current [15,26]. Figure 4(e)–4(h) shows the ΔR histogram after the pulse application for each DW structure as a function of the applied current density. The histogram is taken for the applied field values in the range of $-10 < H_B < 10$ Oe. At higher current densities, the probability of observing transformations becomes higher and more states are observed, which is likely due to thermal effects. Given the ease with which DW transformations take place, we conjecture that the similarity of the depinning currents at low fields, regardless of the initial DW state, is because the DWs may be transformed under current to the same DW state when they depin.

In summary, we show that resistance measurements can be used not only to detect the presence of a DW but can be used to distinguish both the structure, whether vortex or transverse, and the chirality of DWs trapped in notches in permalloy nanowires. Taking advantage of our ability to prepare and identify DWs of different structures in the same pinning site we demonstrate that the magnetic fields required to depin these four DW states are substantially different yet the threshold current densities to depin these same states are nearly the same in small fields. The former can be well understood by micromagnetic simulations but the latter is more complex since current-induced DW transformations play a critical role in the depinning process and because the depinning current density in low fields is so high that the nanowire temperature is significantly increased.

We thank DMEA for partial support of this work.

*Email address: parkin@almaden.ibm.com

[1] D. A. Allwood *et al.*, Science **309**, 1688 (2005).
[2] S. S. P. Parkin, U.S. Patent No. US 683 400 5 (2004).
[3] L. Berger, J. Appl. Phys. **55**, 1954 (1984).
[4] G. Tatara and H. Kohno, Phys. Rev. Lett. **92**, 086601 (2004).
[5] J. He, Z. Li, and S. Zhang, J. Appl. Phys. **98**, 016108 (2005).
[6] A. Thiaville *et al.*, Europhys. Lett. **69**, 990 (2005).
[7] S. E. Barnes and S. Maekawa, Phys. Rev. Lett. **95**, 107204 (2005).
[8] E. Salhi and L. Berger, J. Appl. Phys. **73**, 6405 (1993).
[9] J. E. Wegrowe *et al.*, Europhys. Lett. **45**, 626 (1999).
[10] J. Grollier *et al.*, Appl. Phys. Lett. **83**, 509 (2003).
[11] N. Vernier *et al.*, Europhys. Lett. **65**, 526 (2004).
[12] C. K. Lim *et al.*, Appl. Phys. Lett. **84**, 2820 (2004).
[13] A. Yamaguchi *et al.*, Phys. Rev. Lett. **92**, 077205 (2004).
[14] M. Klaui *et al.*, Phys. Rev. Lett. **94**, 106601 (2005).
[15] M. Klaui *et al.*, Phys. Rev. Lett. **95**, 026601 (2005).
[16] S. H. Florez, C. Krafft, and R. D. Gomez, J. Appl. Phys. **97**, 10C705 (2005).
[17] A. Yamaguchi *et al.*, Appl. Phys. Lett. **86**, 012511 (2005).
[18] A. Himeno, S. Kasai, and T. Ono, Appl. Phys. Lett. **87**, 243108 (2005).
[19] T. Schrefl *et al.*, J. Magn. Magn. Mater. **175**, 193 (1997).
[20] A. Himeno *et al.*, J. Appl. Phys. **93**, 8430 (2003).
[21] M. Hayashi *et al.*, Phys. Rev. Lett. **96**, 197207 (2006).
[22] We ignore other typically smaller contributions to the DW resistivity [see, for example, A. D. Kent *et al.*, J. Phys. Condens. Matter **13**, R461 (2001)].
[23] M. Bolte *et al.*, Phys. Rev. B **72**, 224436 (2005).
[24] M. R. Scheinfein, LLG Micromagnetic Simulator.
[25] Micromagnetic simulations are performed on a permalloy nanowire of the same size as that used in the experiment. The notch profile is mimicked from atomic force microscopy images. A slowly varying field is applied to move the DW across the notch so as to obtain the total energy of the system as a function of the DW position. The DW potential energy landscape is then obtained from the total energy of the system minus the Zeeman energy.
[26] T. Ishida, T. Kimura, and Y. Otani, Phys. Rev. B **74**, 014424 (2006).